Thermal stability of α-titanium in contact with titanium nitride

Shi-Qing Wang
SEMATECH, 2706 Montopolis Drive, Austin, Texas 78741, and Fairchild Research Center, National Semiconductor, Santa Clara, California 95052

Leslie H. Allen
Materials Science Department, University of Illinois at Urbana, Urbana, Illinois 61801

(Received 1 September 1995; accepted for publication 20 November 1995)

The thermal stability of an α-Ti film in contact with a δ-TiN film in the structure of a TiN/Ti/TiN film stack on SiO_2 substrates was studied by *in situ* sheet resistance (R_s) measurement, Auger electron spectroscopy, glancing angle x-ray diffractometry, cross-sectional transmission electron microscopy, scanning electron microscopy, and atomic force microscopy. It was found that nitrogen dissolves from TiN into Ti between 405 and 474 °C and a significant reaction between Ti and TiN results in the formation of ϵ-Ti_2N in the temperature range of 505–548 °C. © *1996 American Institute of Physics.* [S0021-8979(96)02305-7]

I. INTRODUCTION

In ultralarge-scale integration (ULSI) devices film stack structures such as Ti/TiN or Ti/TiN/Ti are commonly utilized as liners before subsequent deposition of contact/via plugs (i.e., CVD W) and interconnect lines (i.e., PVD Al-Cu alloy) or as wetting layers for planarized conductor plugs/lines (i.e., hot deposited/reflowed PVD Al-Cu alloy). The first Ti layer in the contact liner is used to reduce contact resistance over the Si junction regions (either salicided or nonsalicided) by gettering interface impurities such as oxygen, while TiN is used as an adhesion/diffusion barrier layer. For planarized Al-Cu by hot deposition/reflow, a second Ti layer on top of TiN acts as a wetting layer to facilitate Al-Cu flow. In these applications, the stability of Ti in contact with TiN is very important. For example, there may be undesirable effects if Ti absorbs N from the TiN film at lower temperatures than that at which Ti getters oxygen impurities at the Si junction/Ti interface (oxygen dissolves into Ti-N more slowly than into pure Ti) or that at which Al-Cu starts to flow on Ti (Al is known to reflow well on Ti but not on TiN). Furthermore, the integrity of the adhesion/barrier layer could be questionable if TiN loses a substantial amount of N by its interaction with Ti.

To the best of our knowledge, no systematic study exists on the thermal stability of an *isolated* Ti/TiN interface. If the Ti/TiN interface does exist in some structures, it is usually not free from interference by active foreign elements (other than Ti or TiN) from substrates such as Si in the Si/Ti/TiN structure, from overlayers such as Al in the SiO_2/Ti/TiN/Al structure or from both substrates and overlayers such as Si and Al in the Si/Ti/TiN/Al structure. These foreign elements are not inert but rather active in the temperature range around which the Ti/TiN interface stability becomes questionable. In this paper, we report a detailed investigation into the reaction starting temperature and the reaction phase formation of a stand-alone α-Ti/δ-TiN interface on an inert substrate without any overlayer containing foreign elements.

II. EXPERIMENT

All of the studies were conducted on unpatterned 200 mm blanket wafers. The substrates were 600 nm of thermally grown SiO_2 on Si(100).

A Varian M2000/8 cluster sputter deposition system with five modules was used for this work. The system was allowed to pump down to a base pressure of less than 5×10^{-8} Torr. The Ti and TiN films were made by sputtering a Tosoh Ti target (purity level: 99.995%) in Ar gas (purity level: <10 ppb for each impurity such as H, CO, CO_2, H_2O, particle, etc.) and N_2 gas (purity level: <10 ppb for each impurity), respectively. A collimator was inserted between the target and the substrate for all of the depositions. The collimator cell has a hexagonal shape and the cell's diameter and depth are both 5/8 in. The depositions were performed through an *in situ* sequence of degas, sputter etch, and deposition of trilayer TiN/Ti/TiN film stack in one single module without breaking vacuum. Detailed recipes for these processing steps are listed in Table I.

In ULSI multilevel metal applications, the thickness combination of the bilayer Ti/TiN liner structure is typically 7.5 nm/12 nm at the bottom of the contact/via for CVD W plug applications. With an assumption of 30% bottom step coverage, a 25 nm/40 nm thickness combination on the field is required for Ti/TiN. The targeted overall Ti/TiN thickness ratio (100 nm/2×80 nm) for this study reflects this combination. Ti is known to react with SiO_2 and to absorb impurities such as oxygen more readily than TiN. Therefore, a sandwich structure is used here, where the TiN film under Ti prevents the interaction of Ti with the SiO_2 substrate at elevated temperatures while the surface TiN protects Ti from direct exposure to air.

Four point probe sheet resistance (R_s) on samples were measured *in situ* inside a vacuum furnace. The furnace had a base pressure of 2×10^{-8} Torr. However, during temperature ramp, the pressure eventually reached 3×10^{-7} Torr. The first R_s measurement was at 20 °C inside the vacuum furnace and then *in situ* R_s was continuously monitored while the furnace was ramped up to various maximum temperatures between 405 and 624 °C at a ramp (both heating and cooling) rate of 1.5 °C/min. Fresh unannealed samples were used for each temperature ramp with *in situ* R_s measurements. The four probes were configured in a square shape with a 5 mm spacing. A constant 5 mA current was applied to two adjacent probes, and the voltage averaged over two measurements

 0021-8979/96/79(5)/2446/12/$10.00

TABLE I. Processing parameters for the deposition of trilayer TiN/Ti/TiN film stack on the SiO_2 substrate.

Process	Target thickness (nm)	Time (s)	Temp. (°C)	Power (kW)	Ar pressure (mTorr)	Bias (V)
1. Degas	n/a	40	250	n/a	2–3	n/a
2. Sputter etch	10 SiO_2 removal	60	250	0.167	5	−700
3. Deposition: collimated						
Film	Target thickness (nm)	Temp. (°C)	Power (kW)	Pressure (mTorr)	% N (N_2:Ar, sccm)	Bias (V)
TiN	80	250	13.0	3.7	100(80:0)	0
Ti	100	250	8.0	2.0	0(0:21)	0
TiN	80	250	13.0	3.7	100(80:0)	0

while currents of both polarities was monitored every 20 s on the two remaining probes.

Auger analysis was performed with a Perkin Elmer, PHI 670 Scanning Auger Nanoprobe. The AES electron beam was operated at 10 kV and 10 nA. It was scanned over a 30 μm×30 μm area. 3 keV Ar ions were used for sputter etch with an equivalent SiO_2 sputter rate of 7.86 nm/min, rastered over a 2 mm×2 mm area at 50° incidence from the sample surface normal. Zalar rotation was applied during the sputter etch to improve the depth resolution. Quantitative Auger analysis of the Ti-N system is hindered by the spectral overlap of the Ti($L_3M_{2,3}M_{2,3}$) peak and the only major N peak, N($KL_{2,3}L_{2,3}$). To compensate for this overlap, approximate atomic concentrations of the Ti-N system were calculated from the peak-to-peak $dN(E)/d(E)$ Auger signal intensity depth profile data using a subtract-and-weight data massage program written in the PHI-Matlab environment. The sensitivity factors for all elements in this program were calibrated to Rutherford backscatting (RBS) data. The depth scale is reported in nm SiO_2 sputter equivalent determined from the sputter time.

All x-ray diffractometry (XRD) scans were run at room temperature on a Rigaku DMAX diffractometer having parallel beam thin-film optics and using a monochromatic Cu K_α radiation source. The parallel beam optics permit the incident x rays to strike the thin-film sample at a glancing angle (1.5°) so that a maximum area could be irradiated. The scans allowed the detection of 2θ values from 20° to 90°, which correspond to d spacings from 4.439 to 1.090 Å. The positions and the net intensities (with the background subtraction) of diffraction peaks in the XRD scans were determined and then compared with data from the ICDD-JCPDS standard powder diffraction file of the known phases containing Ti and N. These phases are α-Ti (5-0682: hexagonal, hP2, $P6_3/mmc$), ϵ-Ti_2N (17-386: tetragonal, tP6, $P4_2/mnm$; and 23-1455: tetragonal, tI16, $I4_1/amd$), δ-TiN (38-1420: cubic, cF8, Fm3m), and ζ-Ti_4N_{3-x} (39-1015: rhombohedral, R3m). β-Ti(cubic, cI2, Im3m) was not included since it only exists above 882 °C. Another old version of TiN phase (6-0642: cubic, cF8, Fm3m) was excluded because the TiN sample used in that study contained Zr and the study was conducted in 1953. The file was replaced by TiN (38-1420), which was compiled based on several new studies up to 1987.

Bright-field transmission electron microscopy (TEM) micrographs of cross-section views were taken on a Philips CM30 using an accelerating voltage of 300 kV. Cross-sectional samples were prepared using mechanical thinning, dimpling and ion-beam milling. The scanning electron microscopy (SEM) used for the surface morphology observation was an Amray 1845 FE field emission microscope with an accelerating voltage of 15 kV and a tilt angle of 60°.

A Digital Instruments NanoScope III with a Tapping Mode Atomic Force Microscope was used for atomic force microscopy (AFM) analysis. The area scanned was 1.0 μm ×1.0 μm and 20 μm×20 μm. The data were flattened and planefit, and then the roughness values were calculated.

III. RESULTS

A. *In situ* R_s measurement

The sheet resistance (R_s) of the TiN/Ti/TiN film stack system, which acts as three resistors in parallel, was measured *in situ* during annealing. All samples were annealed at a ramp rate of 1.5 °C/min to a given maximum temperature (T_{max}) and then cooled at the same rate of −1.5 °C/min to ambient conditions. Six different samples were annealed to various values of T_{max}: 405, 474, 505, 548, 564, and 624 °C. Additional analysis of the R_s data includes the determination of the temperature coefficient of resistivity (TCR) for both heating and cooling cycle by measuring the average slope of the R_s versus temperature data over the range of 20–200 °C.

The results of the *in situ* R_s measurement on the TiN/Ti/TiN film stacks can be partitioned into three main temperature ranges. For the anneal to T_{max}=405 °C, the system appeared to be stable. The value of R_s increased linearly with the increasing temperature, and the cooling curve was completely reversible from the heating curve [Fig. 1(a)]. The positive slope of this linear reversible curve was measured to be +1890 ppm/°C (normalized to the R_s value at 20 °C). Visual inspection showed that the sample remained the reddish color of TiN after the anneal. The second temperature range was from 474 to 505 °C. Although the sample color remained reddish when T_{max} was increased to 474 °C, an

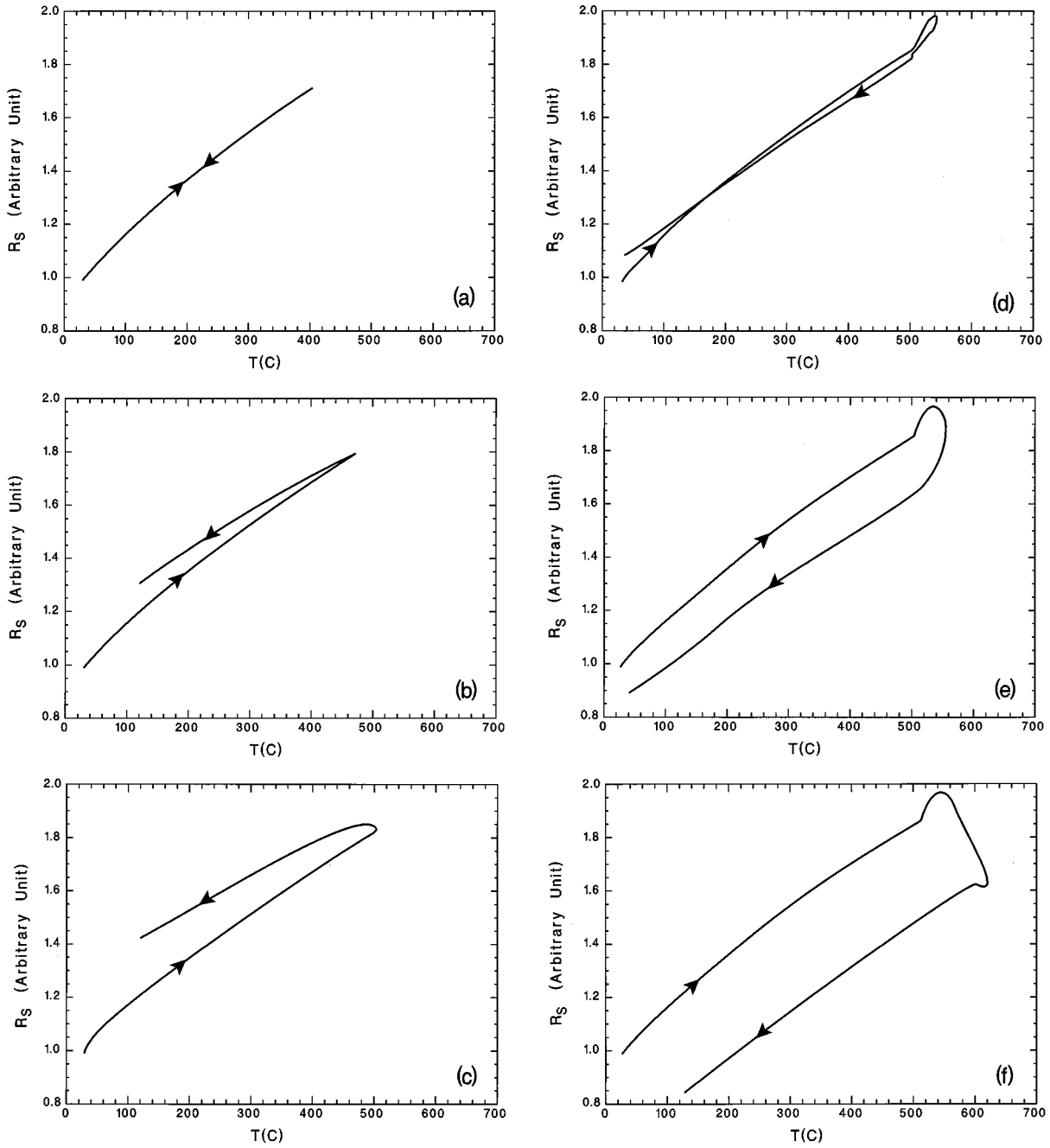

FIG. 1. *In situ* R_s curves on the $Si/SiO_2/TiN/Ti/TiN$ samples measured inside a vacuum furnace ramped up to maximum temperatures of (a) 405 °C, (b) 474 °C, (c) 505 °C, (d) 548 °C, (e) 564 °C, and (f) 624 °C with a ramp rate of 1.5 °C/min. The arrows indicate the heating and cooling curves.

irreversible change in R_s curves occurred. As shown in Fig. 1(b), the cooling curve moved up above the heating curve. In addition, there was a gradual decrease in the slope for both curves with the increasing temperature. At a fixed temperature, the slope for the cooling curve is smaller than that of the heating curve. The sample color remained unchanged but irreversibility became more profound for the anneal to $T_{max}=505$ °C [Fig. 1(c)], where the cooling curve moved further up above the heating curve. Therefore, some interaction had started between $T_{max}=405$ °C and $T_{max}=474$ °C.

In the third temperature range, anneals up to $T_{max}=548$, 564, and 624 °C caused both the sample color to change from reddish to yellowish and the R_s value to vary irreversibly [Figs. 1(d)–1(f)], indicating significant reactions occurred between $T_{max}=505$ °C and $T_{max}=548$ °C. In Fig. 1(d) corresponding to $T_{max}=548$ °C, a section of the *in situ* R_s heating curve from 505 to about 540 °C, which had a steeper positive slope than the section of the curve below 505 °C, was found. The cooling curve for $T_{max}=548$ °C almost traced the heating curve back to room temperature. For $T_{max}=564$ and 624 °C, the heating curves had the same trend as that for $T_{max}=548$ °C with an initial linear region up to 505 °C followed by a section of increased positive slope beyond 505 °C. When the temperature was raised above 540 °C approximately, the heating curves dropped with a large negative slope. The cooling curves moved progressively down

TABLE II. The sample color as observed by visual inspection and the reversibility of the *in situ* R_s curves of the samples annealed to various maximum temperatures (T_{max}) at a ramp rate of 1.5 °C/min.

T_{max} (°C)	Color	*In situ* R_s curve reversibility
405 and below	Reddish	Yes
Between 474 and 505	Reddish	No
Between 548 and 624	Yellowish	No

below the heating curves with the increasing T_{max}. It should be noted that the nearly overlapping heating and cooling curves for T_{max}=548 °C does not necessarily indicate that little reaction had occurred during the anneal. When all the *in situ* R_s data were analyzed together, it was found that the cooling curves changed their positions relative to the heating curves from above them as in the case of T_{max}=474 and 505 °C to below them as in the case of T_{max}=564 and 624 °C. The cooling curve for T_{max}=548 °C happened to swing across, and almost overlapped, the heating curve during this transition.

It is interesting to observe that all of the cooling curves had an identical slope for T_{max}=474 °C and above. This slope is smaller than that of the heating curves at a fixed temperature. T_{max}=505 °C is very close to the maximum temperature at which the cooling curve was most distant above the heating curve. Table II briefly summarizes the three different stages of those observations.

From *in situ* R_s measurements and visual inspections, the samples annealed to T_{max}=505 and 624 °C, together with an unannealed sample, would represent the characteristics of each reaction stages. As a result, the more detailed analysis reported below were concentrated on these three samples.

B. Cross-sectional TEM

Three samples, one unannealed ($Si/SiO_2/TiN/Ti/TiN$) and two annealed to T_{max}=505 and 624 °C, were analyzed by cross-sectional TEM.

TEM micrograph [Fig. 2(a)] indicated that the unannealed sample had a configuration of SiO_2/TiN(66 nm)/Ti(76 nm)/TiN(80 nm) instead of the targeted SiO_2/TiN(80 nm)/Ti(100 nm)/TiN(80 nm) structure. The bottom TiN film (next to the SiO_2 substrate) had a columnar grain structure with a sharp and smooth TiN/Ti interface. However, the top TiN layer had a block grain structure and the Ti/TiN interface was not well defined and relatively rough. The grain structure of the top TiN layer was also similar to that of the Ti layer. Therefore, the grain structure of the TiN films are substrate dependent. The two-dimensional (parallel to the sample surface) equiaxial grain sizes of bottom TiN and Ti films were measured to be approximately 10 and 100 nm, respectively. The grain size for the top TiN film could not be identified clearly due to the excessive thickness in that region of the unannealed cross section sample. However, some evidence suggested that the grain size of this film was slightly greater than that of the Ti film. A composite electron diffraction pattern (not shown) from the combined TiN/Ti/TiN layers of the cross-section sample showed preferred orientations of Ti(110) perpendicular to, and TiN(200) both perpendicular and parallel to, the surface of the sample. TiN(111) was also found to be oriented preferentially at an angle of 35.15° with respect to the sample surface. Due to instrumental limits for selecting a sufficiently small sample area, preferred orientation identification of the separate TiN films was not possible by electron diffraction.

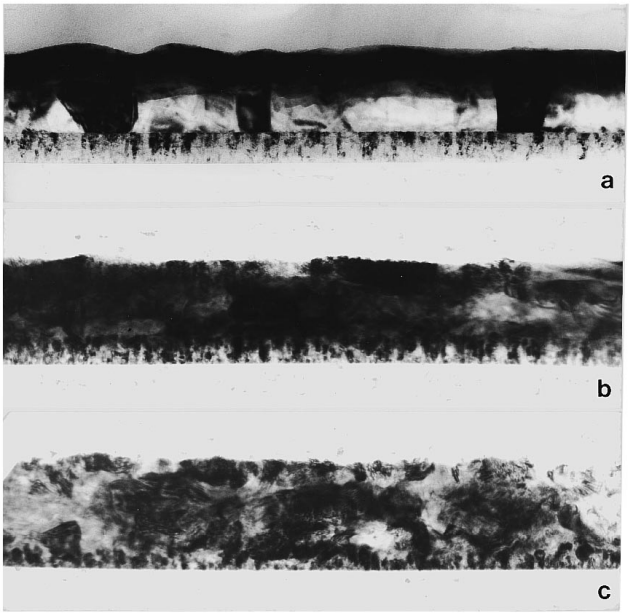

FIG. 2. Cross-sectional TEM micrographs of the $Si/SiO_2/TiN/Ti/TiN$ samples: (a) unannealed, and annealed to maximum temperatures of (b) 505 °C and (c) 624 °C.

In the sample annealed to T_{max}=505 °C, the bottom TiN film was still present and its thickness change was minimal [Fig. 2(b)]. However, the bottom TiN/Ti interface was not as smooth and sharp as that of the unannealed sample. Local grain structure modification due to an interaction could be observed in the bottom TiN film next to the bottom TiN/Ti interface. The Ti grains appeared to have become laminar in shape, lying parallel to the sample surface. Furthermore, the Ti/top TiN interface became less visible. Compared to the unannealed sample, the orientation was less preferred (diffraction pattern is not shown).

Further anneal to T_{max}=624 °C caused a significant growth in the thickness of the middle layer, where Ti was initially located [Fig. 2(c)]. Although the top TiN appeared to be absent, a bottom film below the middle layer, which had a similar grain structure as, and 25% of, the thickness of the original bottom TiN film in the unannealed sample, could still be observed. The anneal to T_{max}=624 °C also resulted in a reduction of texture (diffraction pattern is not shown) as compared with the sample annealed to T_{max}=505 °C.

It should be noted that the quality of these cross-sectional TEM micrographs are not ideal. During TEM sample preparation, peeling occurred due to poor adhesion between the bottom TiN film and the SiO_2 substrate before a desired cross-sectional TEM sample thickness could be obtained. A thin Ti adhesion layer at the SiO_2/bottom TiN interface could prevent such peeling.

TABLE III. The estimated thicknesses (nm SiO_2 sputter equivalent) and the N/Ti concentration ratios for the three layer structure, as detected by AES, of the unannealed sample TiN(bottom, 66 nm)/Ti(middle, 76 nm)/TiN(top, 80 nm) and those annealed to maximum temperatures (T_{max}) from 405 to 624 °C. The SiO_2/TiN interface width (defined as 16% to 84% max signal for the Ti+N peak) is also listed to gauge the maximum loss of depth resolution due to sputter etch roughening.

	Layer thickness (nm SiO_2 equivalent)				N/Ti ratio		
T_{max} (°C)	Top	Middle	Bottom	SiO_2/TiN Interface width	Top	Middle	Bottom
Unannealed	149	150	145	210	1.12	<0.01	1.12
405	149	149	143	230	1.12	<0.01	1.12
474	148	148	143	260	1.12	0.03	1.07
505	149	126	146	230	1.11	0.08	1.02
548	122	200	144	290	1.08	0.51	0.90
564	96[a]	374[a]	87[b]	380[a]	1.08	0.57	0.86
624	86	260	86	260	1.03	0.64	0.84

[a]There appears to have been a problem with the sputter rate calibration for the sample annealed to T_{max}=564 °C.

C. AES

Seven samples, which included an unannealed Si/SiO_2/TiN/Ti/TiN sample and the samples annealed to T_{max}=405, 474, 505, 548, 564, and 624 °C, were analyzed by Auger electron spectroscopy (AES). Table III summarizes the estimated thicknesses and the N/Ti concentration ratios for the three layers of each sample. Figure 3 only shows three AES spectra, one for the unannealed sample and the other two for the samples annealed to T_{max}=505 and 624 °C. It should be noted that O and C concentrations in all samples are within the AES signal noise level.

From Table III and Fig. 3, a clear three-layer structure and the corresponding sharp interfaces existed for the unannealed sample [Fig. 3(a)] and the three samples annealed to T_{max}=405 (figure not shown), 474 (figure not shown), and 505 °C [Fig. 3(b)]. For T_{max}=405 °C, there was no change in the stoichiometries of either TiN films as compared to the unannealed sample. However, when T_{max} was increased to 474 and 505 °C, the N/Ti ratio of the middle Ti layer increased slightly from <0.01 for the unannealed sample and the sample annealed to T_{max}=405 °C to 0.03 and 0.08, respectively. Correspondingly, the N/Ti ratio of the bottom TiN layer decreased slightly (1.07 and 1.02, respectively, from a value of 1.12), although little change in this ratio was observed in the top TiN films. Therefore, some interactions between the films had occurred. It should be noted that even with decreases, the N/Ti ratios of the bottom TiN layers are still larger than one for T_{max}=474 and 505 °C.

Further increases in T_{max} to 548 °C and above resulted in large increases in the thicknesses and the N/Ti ratios of the middle layers and significant decreases in the N/Ti ratios of the bottom TiN films as compared to those of the sample annealed to T_{max}=505 °C (Table III), confirming the occurrence of a significant reaction between Ti and TiN in the temperature range of 505–548 °C. The N/Ti ratios of the bottom TiN films were all smaller than one. The decreases in the N/Ti ratios were also observed in the top TiN films. However, these ratios remained larger than one. Furthermore, the AES spectra for the samples annealed to T_{max}=548 °C and above looked identical [only one spectrum corresponding to T_{max}=624 °C is shown in Fig. 3(c)], indicating the reaction has slowed to completion in this temperature range. Although the three-layer structure became much less clear and the locations of the interfaces were difficult to identify, growth of the middle layer, where Ti was initially located, at the expense of two neighboring TiN films, was apparent. These findings are consistent with the results obtained from *in situ* R_s measurements and cross-sectional TEM observations (sections A and B, respectively).

AES analysis suggests Ti reacts with the bottom TiN layer next to the SiO_2 substrate more easily than it does with the top TiN film. This was evidenced by the faster drop in the N/Ti ratio as a function of T_{max} for the bottom TiN layer than for the top TiN film. Furthermore, the AES spectrum for the sample annealed to T_{max}=624 °C shows that a thin layer of TiN (N/Ti ratio is 1.03 with a 86 nm SiO_2 sputter equivalent) still exists at the surface, while it is much less convincing that any TiN (N/Ti ratio is only 0.84) is present next to the SiO_2 substrate. This finding appears to be different from the results obtained by the cross-sectional TEM analysis (section B). From TEM analysis, a gradually thinned bottom film in annealed samples, which has the same location and a similar grain structure as the original bottom TiN film in the unannealed sample, was more visible than the top TiN film. It is possible that the invisibility by TEM of the top TiN film in the annealed samples is caused by the similarity in grain structure of this film to the middle layer, where the Ti film is initially located. Furthermore, the absence of grain structure modification in the remaining bottom film in the annealed samples, as observed by TEM, does not necessarily exclude the occurrence of a reaction by, for example, losing nitrogen from this film.

Since the unannealed sample has a configuration of Si/SiO_2/TiN(66 nm)/Ti(76 nm)/TiN(80 nm) from the cross-sectional TEM analysis, the sputter rates are calculated to be 3.58, 3.98, and 4.22 nm/min for the bottom TiN film, Ti film, and the top TiN layer, respectively. The SiO_2 sputter equivalent can not be translated directly to real thicknesses since the sputtering rates are different. This is true even for the TiN layers with the same N/Ti ratio but different grain structures

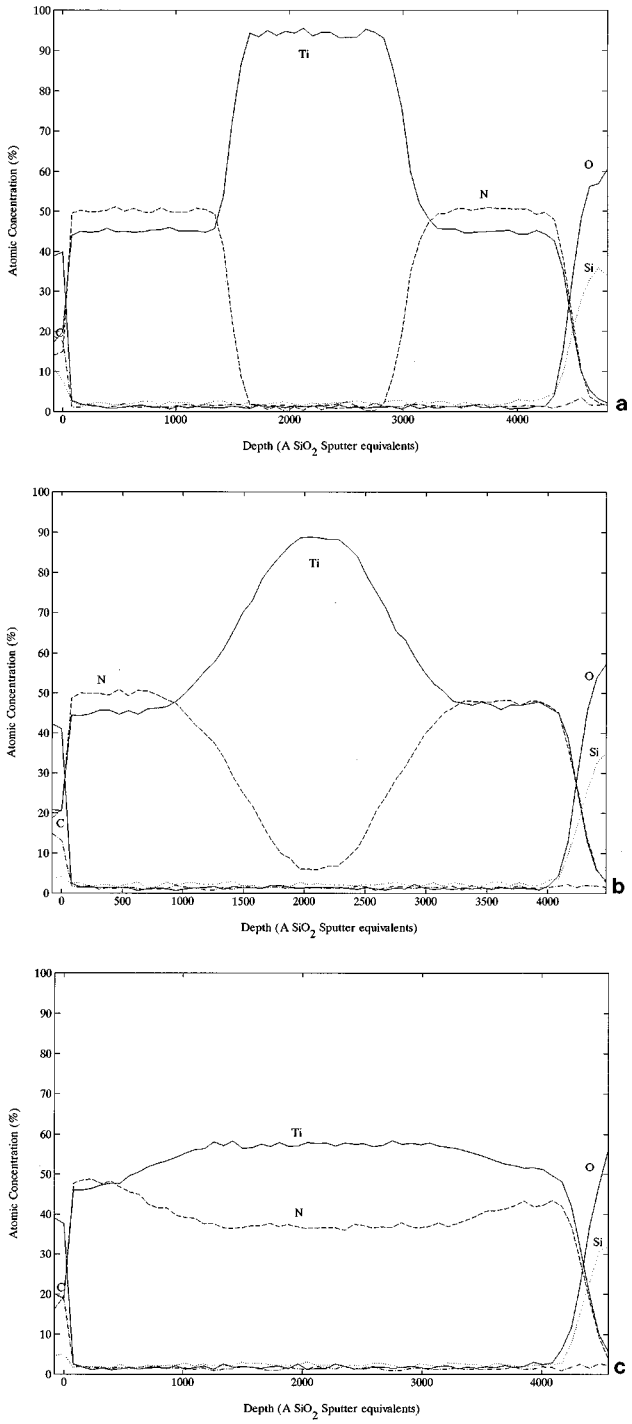

FIG. 3. AES spectra of the $Si/SiO_2/TiN/Ti/TiN$ samples: (a) unannealed, and annealed to maximum temperatures of (b) 505 °C, and (c) 624 °C.

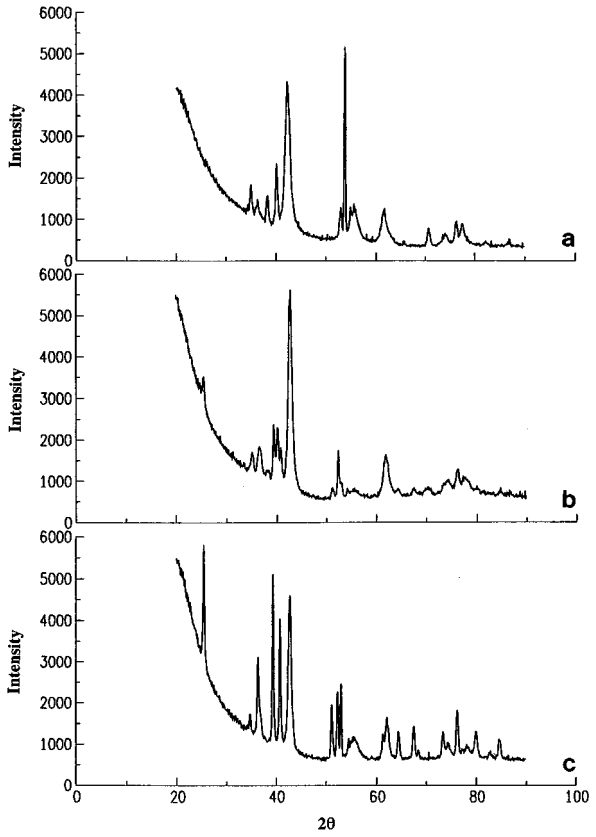

FIG. 4. XRD spectra of the $Si/SiO_2/TiN/Ti/TiN$ samples: (a) unannealed, and annealed to maximum temperatures of (b) 505 °C and (c) 624 °C.

in the unannealed sample. For the TiN thickness ratio of the top film to the bottom layer, TEM shows 80/66=1.21 while AES gives 149/145=1.03. Therefore, the AES sputter rate is 17% higher for the top TiN film than for the bottom TiN layer for that sample.

D. XRD

Figure 4 shows the glancing angle XRD spectra on an unannealed sample [Fig. 4(a)], and the samples annealed to T_{max}=505 [Fig. 4(b)] and 624 °C [Fig. 4(c)]. The strongest peak [135% relative intensity with respect to the second strongest experimental TiN(200) peak with a 100% relative intensity, 2θ=42.33° and d=2.135 Å] located at 2θ=53.86°, corresponding to a value of d spacing 1.702 Å, in the XRD spectrum for the unannealed sample was due to scattering from the substrate [Fig. 4(a)]. This peak was not present in the XRD scans for the samples annealed to T_{max}=505 and 624 °C. The holder used for the unannealed sample for XRD analysis was different from, and larger than, that used for the two annealed samples due to the larger size of the unannealed sample.

A list of d spacings and the relative intensities of the diffraction peaks (normalized to the intensity of the strongest peak in each scan) from these experimental XRD scans is given in Table IV. Also included in the table are the complete (without skipping) d spacings listed in the order of decreasing values and their relative intensities from the ICDD-JCPDS standard powder diffraction file of the phases α-Ti(5-0682), δ-TiN(38-1420), and ϵ-Ti_2N(17-386). The phases Ti_2N(23-1455) and ζ-Ti_4N_{3-x}(39-1015) are excluded in the table because no match could be found. It was found that every single diffraction peak in the experimental XRD scans for the unannealed sample, and the samples annealed to T_{max}=505 and 624 °C could be matched within a reasonable error by d spacings of one or two of the α-Ti(5-0682), δ-TiN(38-1420), and ϵ-Ti_2N(17-386) phases in the ICDD-JCPDS file. The opposite claim is true, too. Every single d spacing of the three phases reported in the file could be posi-

TABLE IV. List of d spacings and the relative intensities of the diffraction peaks (normalized to the intensity of the strongest peak) from the experimental XRD scans on the unannealed sample, and the samples annealed to T_{max}=505 and 624 °C. Also included in the table are the complete (without skipping) d spacings listed in the order of decreasing values and the relative intensities from the ICDD-JCPDS powder diffraction file of the phases α-Ti (5-0682), δ-TiN (38-1420), and ϵ-Ti_2N (17-386). The scans allowed the detection of 2θ values from 20° to 90°, which correspond to d spacings from 4.439 to 1.090 Å, respectively. (a), (b), and (c) indicate a possible multiple match of an experimental d spacing to those of one or two phases reported in the file.

	Powder diffraction d spacing (Å); relative intensity (%)			Experimental d spacing (Å); relative intensity (%)		
(hkl)	α-Ti (5-0682)	δ-TiN (38-1420)	ϵ-Ti_2N (17-386)	Unannealed	505 °C	624 °C
(110)			3.500;20		3.488;13	3.498;73
(101)			2.586;10			3.581;9
(010)	2.557;30			2.556;20	2.558;9	
(200)			2.473;80	[a]2.465;11	2.459;14	2.471;48
(111)		2.449;72		[a]2.465;11	2.459;14	2.471;48
(002)	2.342;26			2.344;16	2.345;3	
(111)			2.292;100		2.288;27	2.288;100
(011)	2.244;100			2.244;38	2.246;28	
(210)			2.211;50			2.211;69
(200)		2.121;100		2.135;100	2.117;100	2.114;88
(211)			1.788;50		1.791;5	1.785;33
(220)			1.749;50		1.747;24	1.748;41
(012)	1.726;19			1.727;20		1.726;45
(002)			1.517;50			1.512;15
(220)		1.500;45		1.489;18	1.499;21	1.496;25
(110)	1.475;17					
(301)			1.448;80		1.448;4	1.448;16
(311)			1.390;80		1.390;3	1.389;21
(320)			1.371;10			1.372;6
(103)	1.332;16			1.333;12	1.335;3	1.336;2
(202)			1.293;50		1.292;6	1.291;14
(311)		1.279;19		[b]1.282;7		1.277;5
(200)	1.276;2			[b]1.282;7		1.277;5
(212)			1.251;50	[c]1.248;15	1.250;11	1.249;25
(321)			1.250;50	[c]1.248;15	1.250;11	1.249;25
(112)	1.247;16			[c]1.248;15	1.250;11	1.249;25
(201)	1.233;13			1.232;14	1.234;7	

tively identified within a reasonable error by one diffraction peak in the experimental XRD scans from the three samples. The only exception is for Ti(110) (2θ=63.02°, d=1.475 Å) in the ICDD-JCPDS file. This peak is very close to the strong TiN(220) peak (2θ=61.85°, d=1.500 Å). A careful examination of the TiN(220) diffraction peak (2θ=62.36°, d=1.489 Å) in the experimental XRD scan for the unannealed sample indicates that a weak high angle shoulder exists. It is likely that this shoulder in the TiN(220) peak is from Ti(110).

From the table, it is clear that only α-Ti(5-0682) and δ-TiN(38-1420) phases existed in the unannealed sample.

TABLE V. The lattice parameter values (Å) and their standard deviations (%,1σ) calculated using a least-squares fitting algorithm from the diffraction peaks of the experimental XRD scans on the unannealed sample and the samples annealed to T_{max}=505 and 624 °C. Efforts were made to use at least three peaks that can be uniquely assigned to the phase whose lattice parameters are calculated. The total number of peaks used for the calculation and the number of "unique" peaks among them are given in parenthesis.

	Lattice parameters (a or c) in Å/standard deviation in %, 1σ (total # peaks used/# of unique peaks)		
Sample ID	α-Ti(hexagonal)	δ-TiN(cubic)	ϵ-Ti_2N(tetragonal)
Standard powder diffraction	(5-0682) a=2.950 c=4.686	(38-1420) a=4.2417	(17-386) a=4.9452 c=3.0342
Experimental			
Unannealed	a=2.948/5(6/6) c=4.686/10(6/6)	a=4.230/4(4/2)	Only two non unique peaks
505 °C	a=2.954/9(5/5) c=4.696/19(5/5)	a=4.231/20(3/2)	a=4.946/9(7/7) c=3.031/4(7/7)
624 °C	a=2.958/3(4/2) c=4.718/7(4/2)	a=4.241/3(3/2)	a=4.950/4(10/10) c=3.029/2(10/10)

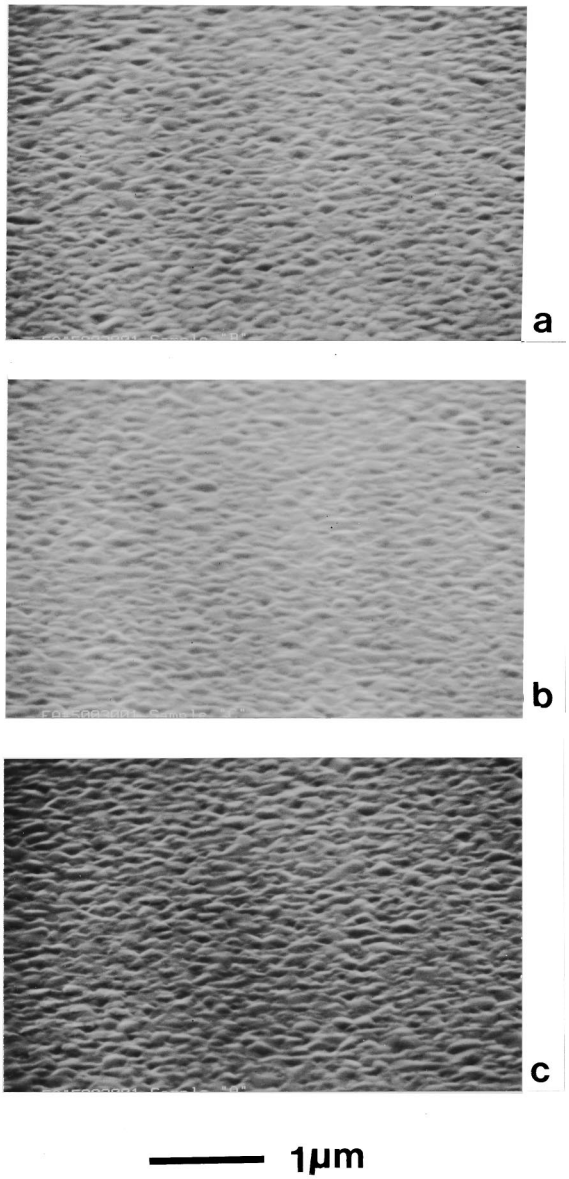

FIG. 5. Surface SEM micrographs of the $Si/SiO_2/TiN/Ti/TiN$ samples: (a) unannealed, and annealed to maximum temperatures of (b) 505 °C and (c) 624 °C.

Annealing to $T_{max}=505$ and 624 °C causes a reaction between Ti and TiN to form ϵ-Ti_2N(17-386). Although the Ti_2N phase was detected by XRD in the sample annealed to $T_{max}=505$ °C, its quantity was small. In Table IV, the relative intensities of the experimental XRD peaks matching the Ti_2N phase for the sample annealed to $T_{max}=505$ °C were significantly smaller than those for the sample annealed to $T_{max}=624$ °C. XRD analysis also indicated that the Ti and TiN phases were not completely consumed in either of the annealed samples. This result is also confirmed by AES analysis, which indicates that the smallest N/Ti ratio is 0.64 (39 at. % N) in the three layer structure of the sample annealed to $T_{max}=624$ °C. The presence of TiN is necessary for the Ti-N mixture with an overall N/Ti ratio greater than approximately 0.5 (34 at. % N), which is the maximum solubility of N in Ti_2N at 624 °C. Furthermore, these ratios do not exclude the possibility of coexistence of Ti in these layers either.

Table V lists the lattice parameter values of α-Ti(5-0682), δ-TiN(38-1420), and ϵ-Ti_2N(17-386) phases calculated from the diffraction peaks corresponding to these phases in the experimental XRD scans on the unannealed sample and the samples annealed to $T_{max}=505$ and 624 °C. The calculation employed a least-squares fitting algorithm with a drift factor for systematic errors from the diffractometer. The results indicate that the lattice parameter a for α-Ti(hexagonal), δ-TiN(cubic), and ϵ-Ti_2N(tetragonal) and the lattice parameter c for α-Ti increase, while c for ϵ-Ti_2N decreases with the increasing T_{max}.

E. SEM and AFM

SEM observations under the same magnification showed very similar surface morphologies [Figs. 5(a), 5(b), and 5(c)] for the unannealed sample Si/SiO_2TiN(66 nm)/Ti(76 nm)/TiN(80 nm) and the samples annealed to $T_{max}=505$ and 624 °C. Small bumps were observed on all three sample surfaces. There is a slight difference in the size of these bumps, with those for the unannealed sample ranging from 100 to 200 nm, and those for the samples annealed to $T_{max}=505$ and 624 °C averaging 200 and 250 nm, respectively. These bumps may not be interpreted as the grains of the surface TiN film. It could be caused by the cumulative roughness of the underlying films. This SEM observation of similarity in surface morphologies for the three samples is also confirmed by AFM measurement (AFM images are not shown), which indicated that all three samples have identical roughness values of 5.0–5.5 nm for both 1.0 μm×1.0 μm and 20 μm×20 μm scan areas. It should be noted that the SiO_2/TiN and bottom TiN/Ti interfaces are flat and smooth for the unannealed sample from the cross-sectional TEM analysis. The surface roughness is, therefore, mainly caused by the films located above the bottom TiN/Ti interface in that sample.

F. Summary of experimental results

Table VI summarizes the results obtained by *in situ* R_s, TEM, AES, XRD, SEM, and AFM. It is clear that *in situ* R_s measurement is the most sensitive technique in detecting the occurance of a change in the TiN/Ti/TiN film stack system. The R_s curve loses reversibility while AES shows a very slight N/Ti ratio change in the Ti and the bottom TiN layers at a T_{max} value as low as 474 °C. Unfortunately, XRD data are not available to show if any small quantity of Ti_2N exists at this temperature. When T_{max} is increased to 505 °C: *in situ* R_s, TEM, AES, and XRD techniques all indicate that an interaction has occurred. However, a triple-layer TiN/Ti/TiN structure is still relatively intact. A significant reaction occurs in the temperature range of $T_{max}=505$–548 °C.

IV. DISCUSSION

A. Thermodynamics

The calculation of how thermodynamically favorable the reaction α-Ti+δ-TiN=ϵ-Ti_2N proceeds is difficult due to the lack of thermodynamic data, especially at elevated tempera-

tures, of the Ti_2N phase. The only reported value for this phase is the molar enthalpy of formation $\Delta H_f^0(298\ \mathrm{K})_{Ti_2N} = -95.0$ kcal/mole at room temperature of 298.15 K.[1] The molar entropy of formation (ΔS_f^0) for the M_2N phases at 298.15 K, where M stands for a refractory metal, is typically $\Delta S_f^0(298\ \mathrm{K})_{M_2N} = -18.7$ cal/K mole based on the data (Cr_2N phase was used as a case study) compiled in the Joint Army Navy Air Force (JANAF) Thermochemical Tables.[2] Therefore, the molar Gibbs free energy for the Ti_2N phase at 298.15 K is $\Delta G_f^0(298\ \mathrm{K})_{Ti_2N} = \Delta H_f^0(298\ \mathrm{K})_{Ti_2N} - T\Delta S_f^0(298\ \mathrm{K})_{Ti_2N} = -89.4$ kcal/mole. It should be noted that the $T\Delta S_f^0(298\ \mathrm{K})_{Ti_2N}$ term is 17 times smaller than the $\Delta H_f^0(298\ \mathrm{K})_{Ti_2N}$ term at 298.15 K. Therefore, a small deviation of the accurate $\Delta S_f^0(298\ \mathrm{K})_{Ti_2N}$ value for the Ti_2N phase from -18.7 cal/K mole will not significantly affect the following thermodynamical calculation for the reaction α-Ti+TiN=Ti_2N at 298.15 K. Combining the $\Delta G_f^0(298\ \mathrm{K})_{Ti_2N}$ value with the molar Gibbs free energies for the phases α-Ti and TiN at 298.15 K, $\Delta G_f^0(298\ \mathrm{K})_{\alpha\text{-Ti}} = 0$ and $\Delta G_f^0(298\ \mathrm{K})_{TiN} = -73.8$ kcal/mole,[3] respectively, the net molar Gibbs free-energy change for the reaction α-Ti+TiN=Ti_2N at 298.15 K can be calculated $\Delta[\Delta G_f^0(298\ \mathrm{K})] = \Delta G_f^0(298\ \mathrm{K})_{Ti_2N} - [\Delta G_f^0(298\ \mathrm{K})_{\alpha\text{-Ti}} + \Delta G_f^0(298\ \mathrm{K})_{TiN}] = -15.6$ kcal/mole. Therefore, the reaction is thermodynamically favorable at 298.15 K.

The next attempt is to calculate the $\Delta(\Delta G_f^0)$ value for the reaction of α-Ti+TiN=Ti_2N at 800 K=526.85 °C, which is close to 505 °C when the early formation of the Ti_2N phase from the Ti/TiN reaction was observed by XRD in this study. From the JANAF data for the M_2N phase, the molar heat capacity of the Ti_2N phase $C_p(T)_{Ti_2N}$ as a function of temperature can be determined, and so can the relation $\Delta C_p(T)_{Ti_2N} = C_p(T)_{Ti_2N} - [2C_p(T)_{\alpha\text{-Ti}} + 1/2C_p(T)_{N_2}]$ as a function of temperature with the known temperature dependent relations of $C_p(T)_{\alpha\text{-Ti}}$ and $C_p(T)_{N_2}$, the molar heat capacities for the α-Ti and N_2 phases, respectively. As a result, the molar Gibbs free energy for the Ti_2N phase at a temperature T, where T is below the melting temperatures of the Ti_2N phase, $\Delta G_f^0(T)_{Ti_2N} = \Delta H_f^0(298\ \mathrm{K})_{Ti_2N} + \int_{298}^{T} \Delta C_p(T)_{Ti_2N} dT - T\Delta S_f^0(298\ \mathrm{K})_{Ti_2N} - T\int_{298}^{T} \times \Delta C_p(T)_{Ti_2N}/T dT$ can also be obtained. At $T=800$ K, $\Delta G_f^0(800\ \mathrm{K})_{Ti_2N} = -80.6$ kcal/mole. This $\Delta G_f^0(800\ \mathrm{K})_{Ti_2N}$ value, together with the molar Gibbs free energies for the phases α-Ti and TiN at 800 K, $\Delta G_f^0(800\ \mathrm{K})_{\alpha\text{-Ti}} = 0$ and $\Delta G_f^0(800\ \mathrm{K})_{TiN} = -62.4$ kcal/mole,[3] respectively, can be used to calculate the net molar Gibbs free energy change for the reaction α-Ti+TiN=Ti_2N at 800 K, $\Delta[\Delta G_f^0(800\ \mathrm{K})] = \Delta G_f^0(800\ \mathrm{K})_{Ti_2N} - [\Delta G_f^0(800\ \mathrm{K})_{\alpha\text{-Ti}} + \Delta G_f^0(800\ \mathrm{K})_{TiN}] = -18.1$ kcal/mole. Therefore, the reaction is also thermodynamically favorable at 800 K. The detailed thermodynamic calculation for the $\Delta G_f^0(800\ \mathrm{K})_{Ti_2N}$ value is beyond the scope of this study and is the subject of another publication.[4]

It is interesting to note $\Delta G_f^0(298\ \mathrm{K})$ and $\Delta G_f^0(800\ \mathrm{K})$ values for either TiN or Ti_2N phase are not significantly different. This confirms the Neumann and Kopp's rule, which states ΔC_p may be assumed to be zero for solid-state alloys

TABLE VII. The values at 20 °C and their source references for the properties on the right-hand side of Eq. (1). Note: (a) The ρ values were measured on separate samples in the $Si/SiO_2/\alpha$-Ti and Si/SiO_2TiN structures, where α-Ti and TiN were deposited using the same parameters to a similar thickness range as those used in this study. Thin film effect is thus included; (b) The t values were measured by TEM in this study; (c) Tsai *et al.* reported that the reactively sputtered TiN films have TCR values varying from 228 to 1355 ppm/°C (Ref. 12), depending on the deposition parameters and the film thickness. The TCR value of the TiN film with the deposition parameters and the thickness closest to those used in this study is chosen in the calculation.

	Ti		TiN	
Properties	Value	Ref.	Value	Ref.
$\rho(\mu\Omega$ cm)	60	9	110	9
t (nm)	76	⋯	146	⋯
TCR (ppm/C)	2800	11	1018	12
CTE (ppm/C)	8.6	10	9.35	13

TABLE VI. Summary of the results obtained by *in situ* R_s, TEM, AES, XRD, SEM, and AFM.

Sample ID	Unannealed	405 °C	474 °C	505 °C	548 °C	624 °C
Color	Reddish	Reddish	Reddish	Reddish	Yellowish	Yellowish
In situ R_s	⋯	Reversible	Irreversible	Irreversible	Irreversible	Irreversible
TEM	3 layer w/ visible int'face	⋯	⋯	Similar to the unannealed, slight grain modification	⋯	Significant thickness change/grain modification
AES	3 layers w/ sharp int'face	3 layers w/ sharp int'face	3 layers, very slight N/Ti change	3 layers, slight N/Ti change	Significant thickness & N/Ti change	Similar to 548 °C
XRD	Ti & TiN coexist	⋯	⋯	Small quantity of Ti_2N forms	⋯	Large quantity of Ti_2N forms
SEM	0.15 μm bumps	⋯	⋯	0.20 μm bumps	⋯	0.25 μm bumps
AFM	5.0 nm roughness	⋯	⋯	5.5 nm roughness	⋯	5.5 nm roughness

or compounds with a coordination lattice. Therefore, the simplified relations $\Delta G_f^0(T)=\Delta H_f^0(298\ \mathrm{K})-T\Delta S_f^0(298\ \mathrm{K})$, where T is below the melting temperatures of the TiN and Ti_2N phases, can be used to obtain the ΔG_f^0 values at elevated temperatures by using their corresponding ΔG_f^0 values at room temperature of 298.15 K.

Thermodynamically unfavorable reactions do not occur. On the other hand, a reaction does not necessarily proceed even if it is favorable thermodynamically. Kinetics is another important factor which governs a solid state reaction. For example, although predicted by thermodynamics as favorable in this study, the reaction of α-Ti+TiN=Ti_2N is not observed at room temperature of 298.15 K. The kinetics are too slow for the reaction to occur at an appreciable rate below 505 °C. At temperatures above 505 °C, the driving force is sufficiently high to sustain a noticeable reaction rate.

B. Reaction mechanism

In the low-temperature range of room temperature to 405 °C, it appears from the data of all the analyses that the δ-TiN/α-Ti/δ-TiN system is stable. The initial interaction between the layers occurs in the temperature range of 405–474 °C, as indicated by the irreversible *in situ* R_s curve [Fig. 1(b)] and a slight N/Ti ratio drop from 1.12 to 1.07 of the bottom TiN layer in the AES spectrum (Table III) for the sample annealed to T_{max}=474 °C. The interaction becomes stronger for T_{max}=505 °C. The *in situ* R_s measurement shows a higher degree of irreversibility [Fig. 1(c)]. Nitrogen, as a moving species, may first diffuse out of the bottom $TiN_{1.12}$ layer into the α-Ti film, forming a graded solid solution of α-Ti(N). This is verified by a significant increase in the lattice parameters a and c and their standard deviation values of the α-Ti phase for T_{max}=505 °C, as compared to those of the unannealed sample (Table V). The formation of a graded α-Ti(N) film is also confirmed by AES analysis. In Fig. 3(b) for T_{max}=505 °C, a gradually decreased nitrogen signal was observed from the depth of 3200 to 2100 in the unit of SiO_2 sputter equivalent. This sloped nitrogen profile is not caused by nonuniform AES sputter etch since the SiO_2/TiN interface width of 230 nm SiO_2 equivalent for T_{max}=505 °C is about the same as 210 nm of the unannealed sample (Table III). The N/Ti ratio of the bottom TiN layer is found to decrease further to 1.02 for T_{max}=505 °C (Table III). However, this ratio changes little for the top TiN film (from 1.12 to 1.11) (Table III). Sample color change does not occur for T_{max}=474 and 505 °C since the visually opaque top $TiN_{1.11-1.12}$ film is not involved in the interaction. Sundgren *et al.* have reported that the electrical resistivity of the α-Ti film increases significantly from approximately 70 $\mu\Omega$ cm for pure α-Ti to 200 $\mu\Omega$ cm at an N/Ti ratio of 0.25.[5] On the other hand, the thickness change of the original α-Ti film is probably minimal by dissolution of small amounts of nitrogen from the bottom TiN layer. Therefore, the metal film stack in the $Si/SiO_2/TiN_{1.12-\delta}/\alpha\text{-Ti}(N)/TiN_{1.12}$ structure, where $0<\delta<0.10$ (Table III), has a higher R_s value than that in the original $Si/SiO_2/TiN_{1.12}/\alpha\text{-Ti}/TiN_{1.12}$ structure at all temperatures, resulting in the cooling curve moving up above the heating curve. The higher T_{max} is in the range of T_{max}=474–505 °C, the more nitrogen dissolves into α-Ti from the original bottom $TiN_{1.12}$ layer and the higher the cooling curve moves up above the heating curve.

When T_{max} is increased further to 548 °C and above, a section of the *in situ* R_s heating curves with an accelerated R_s increase, corresponding to larger positive slopes than that of the section below 505 °C, is observed in a temperature window from 505 to about 540 °C [Figs. 1(d)–1(f)]. The decrease of the N/Ti ratio in the bottom TiN layer has reached such a critical value at about 505 °C that any further loss of nitrogen from this layer into the α-Ti film due to the increasing temperature will transform a significant amount of the $TiN_{1.02}$ phase (Table III) into nitrogen deficient TiN (N/Ti ratio$<$1). On the other hand, the nitrogen concentration in the α-Ti film is not sufficiently high at 505 °C to form a significant amount of the Ti_2N phase. A simple calculation indicates that if nitrogen atoms, which are released from the bottom TiN layer so that its composition changes from $TiN_{1.12}$ to TiN, dissolve into the original α-Ti film, the N/Ti ratio in this film would be about 0.09. This ratio is much smaller than 0.5, the N/Ti ratio for the Ti_2N phase. The TiN phase has a nitrogen deficient homogeneity range down to 41 at. % of nitrogen, corresponding to the N/Ti ratio of 0.69, at 500 °C.[6] The electrical resistivity of the TiN phase in this homogeneity range is known to increase by a factor of 6 with the decreasing nitrogen concentration from 50 to 41 at. %.[7] This explains the existence of a section with an accelerated R_s increase in *in situ* R_s heating curve for T_{max}=548 °C.

Further increases in temperature beyond 540 °C result in decreases in the combined R_s for T_{max}=548 °C and above because the nitrogen concentration in the α-Ti film is sufficiently high at 540 °C for the formation of a significant amount of Ti_2N phase. ϵ-Ti_2N is reported to have an electrical resistivity of $\rho(300\ \mathrm{K})_{Ti_2N}$ = 43.1 $\mu\Omega$ cm at room temperature.[8] This value is lower than those of either α-Ti or δ-TiN films deposited in this study.[9] Therefore, the combined R_s value for the metal film stack in the $Si/SiO_2/TiN_{1.12-\zeta}/Ti_2N(Ti)/TiN_{1.12-\xi}$ structure, where $0.22<\zeta<0.28$ and $0.04<\xi<0.09$ (Table III), is smaller than that of the $TiN_{1.12}/\alpha\text{-Ti}/TiN_{1.12}$ film stacks in the original $Si/SiO_2/TiN_{1.12}/Ti/TiN_{1.12}$ structure at all temperatures, resulting in the cooling curves moving down below the heating curves. With increasing T_{max} in the temperature range of 548 °C and above, more Ti_2N forms and the cooling curve moves down further below the heating curve.

It should be remembered that the original bottom and top TiN films in the unannealed sample have similar thicknesses and identical N/Ti ratios (thicknesses are 149 and 145 nm SiO_2 equivalent, respectively, and N/Ti=1.12 from Table III). The only significant difference is their grain structures (10 nm columnar grains for the bottom TiN film and $>$100 nm block grains for the top TiN film). Since grain boundary diffusion is dominant over lattice diffusion in thin-film reactions, the higher the density of grain boundaries intersecting the TiN/α-Ti interface is in the TiN film, the more paths it provides for nitrogen to diffuse out of TiN layer into α-Ti film and the easier it is for a reaction to occur. This explains

why α-Ti reacts with the bottom TiN layer easier than it does with the top TiN film.

In the practical application where α-Ti/TiN layer is used as a liner in the multilevel interconnect structure of conventional CVD W plug/Al-Cu lines, the Ti layer is usually in contact with the overlaying TiN film. Under the Ti layer, several materials could possibly exist: Si(junction)/(salicide) at the contact bottom, Al-Cu/TiN(ARC) at the via bottom, SiO_2 on the sidewall of contacts and vias, and SiO_2 under interconnect lines. Ti is known as a good oxygen getterer. As a result, oxygen could dissolve into Ti from the surface regions of Si(junction)/(salicide) and Al-Cu/TiN(ARC), or from SiO_2 below the reaction starting temperature (405–474 °C) between α-Ti and TiN reported above, where α-Ti is separated from any oxygen source by another layer of TiN. This absorption of oxygen in the α-Ti layer could significantly postpone the interaction or reduce the reaction kinetics in the α-Ti/TiN structure. The higher the oxygen concentration is in the α-Ti layer, the slower the reaction proceeds.

The calculation from the diffraction peaks in the experimental XRD scans on the unannealed sample and the samples annealed to $T_{max}=505$ and 624 °C indicate that the lattice parameter a for α-Ti(hexagonal), δ-TiN(cubic), and ϵ-Ti_2N(tetragonal) and the lattice parameter c for α-Ti(hexagonal) increase, while c for ϵ-Ti_2N(tetragonal) decreases with the increasing T_{max} (Table V). These lattice parameter changes are mainly caused by the nitrogen dissolution into the corresponding α-Ti, TiN, and Ti_2N phases. The higher T_{max} is, the more nitrogen dissolves into these phases. The qualitative trends of these parameter changes with the increasing content of nitrogen dissolution observed in this study are consistent with those reviewed by Wriedt and Murray (see Fig. 4, Table 4, and Fig. 5 of Ref. 6).

It appears confusing that the mechanism for the α-Ti+TiN=Ti_2N reaction is nitrogen dissolution from the TiN layer into the α-Ti film, while XRD lattice parameter measurements indicate that increasing amounts of nitrogen dissolve into the TiN grains with the increasing T_{max}. Some nitrogen in a polycrystalline TiN layer, especially in a nitrogen-rich TiN layer with an overall N/Ti ratio greatly exceeding one, could precipitate at the TiN grain boundaries. At elevated temperatures, these nitrogen atoms could move into the TiN grains and diffuse out of the TiN layer into the α-Ti film at the same time. TiN grains themselves also release nitrogen when they are transformed into Ti_2N at elevated temperatures. These released nitrogen atoms may move into the remaining TiN grains and diffuse into the α-Ti film simultaneously, too. Therefore, the reaction can still cause all of the lattice parameters to change for the α-Ti, Ti_2N, and TiN phases, as observed in this study.

Based on the published data of the relations between the lattice parameters and the content of nitrogen dissolution in the bulk α-Ti, Ti_2N, and TiN phases,[6] it is possible to quantitatively extrapolate, using the lattice parameter changes from the experimental XRD scans in this study, the content of nitrogen dissolution in these phases for the samples annealed to $T_{max}=505$ and 624 °C and compare them to the experimental results of nitrogen content by AES to determine the individual amount of coexisting phases in the different layers of the sample. For example, in this study the lattice parameter a for the α-Ti film of the unannealed sample was 2.948 Å (Table V) at a N/Ti ratio of <0.01 (<1 at. % N, Table III). For the sample annealed to $T_{max}=505$ °C, the Ti lattice parameter a increased to 2.954 Å (0.2% increase, Table V). From Ref. 6, a of Ti is 2.9505 Å at 1 at. % N. An increase in a by 0.2% increases its value to 2.956 Å, which corresponds to 4 at. % N in Ti.[6] However, the experimental AES result shows an overall N/Ti ratio of 0.08 (7 at. % N, Table III) in the middle layer, where Ti is located initially, for the sample annealed to $T_{max}=505$ °C. This indicates that the phase Ti-4 at. % N coexists with Ti_2N phase in this middle layer. It should be noted that the existence of the Ti_2N phase in the sample annealed to $T_{max}=505$ °C is confirmed by XRD but the location of the phase is not determined. A simple calculation shows that, if Ti-4 at. % N coexists with Ti_2N in the middle layer with an overall 7 at. % N for the sample annealed to $T_{max}=505$ °C, the molecular ratio of Ti-4 at. % N to Ti_2N would be approximately 9.

C. Temperature coefficients of resistivity (TCR)

When samples with the δ-TiN/α-Ti/δ-TiN film stacks on inert SiO_2 substrates are annealed to $T_{max}=405$ °C, the *in situ* R_s measurement shows a complete reversibility between the heating and cooling curves and AES analysis indicates that no reaction occurs between α-Ti and TiN. The results imply that α-Ti or TiN grain growth is negligible during the anneal. If such grain growth is significant without any reaction between α-Ti and TiN, the *in situ* R_s cooling curve should move down below the heating curve. The absence of α-Ti or TiN grain growth under anneal to $T_{max}=405$ °C is consistent with the refractory (high melting temperature) nature of these two metals ($T_{melt,\alpha\text{-Ti}}=1668$ °C and $T_{melt,TiN}=2930$ °C, respectively).[10]

The other characteristics of the *in situ* R_s curves is their linear increase with increasing temperature with a common positive slope of +1890 ppm/C (normalized to the R_s value at 20 °C), when samples are annealed to $T_{max}=405$ °C. In the absence of reaction and grain growth, the value of this normalized slope is determined by the electrical resistivity (ρ), the film thickness (t), the temperature coefficients of resistivity (TCR), and the coefficients of thermal expansion (CTE) of the α-Ti and TiN films in the following equation:

$$(1/R_s)(dR_s/dT)=[1/R_{s,\alpha\text{-Ti}}(\mathrm{TCR}_{\alpha\text{-Ti}}-\mathrm{CTE}_{\alpha\text{-Ti}})+1/R_{s,\mathrm{TiN}}(\mathrm{TCR}_{\mathrm{TiN}}-\mathrm{CTE}_{\mathrm{TiN}})]/[1/R_{s,\alpha\text{-Ti}}+1/R_{s,\mathrm{TiN}}]$$
$$=[\rho_{\mathrm{TiN}}t_{\alpha\text{-Ti}}(\mathrm{TCR}_{\alpha\text{-Ti}}-\mathrm{CTE}_{\alpha\text{-Ti}})+\rho_{\alpha\text{-Ti}}t_{\mathrm{TiN}}(\mathrm{TCR}_{\mathrm{TiN}}-\mathrm{CTE}_{\mathrm{TiN}})]/[\rho_{\mathrm{TiN}}t_{\alpha\text{-Ti}}+\rho_{\alpha\text{-Ti}}t_{\mathrm{TiN}}], \quad (1)$$

where R_s, $R_{s,\alpha\text{-Ti}}$, and $R_{s,\text{TiN}}$, are the sheet resistances of the total TiN/α-Ti/TiN stack, the middle α-Ti layer and the combined TiN films (the electrical and thermal properties of the bottom and top TiN films are assumed to be the same), respectively, $(1/R_s)(dR_s/dT)$ is the normalized slope of the linear *in situ* R_s vs temperature curve, $\text{TCR}_{\alpha\text{-Ti}}$ and TCR_{TiN} are the temperature coefficients of resistivity, and $\text{CTE}_{\alpha\text{-Ti}}$ and CTE_{TiN} are the coefficients of thermal expansion for the α-Ti and TiN films, respectively. Relations $R_{s,\alpha\text{-Ti}} = \rho_{\alpha\text{-Ti}}/t_{\alpha\text{-Ti}}$ and $R_{s,\text{TiN}} = \rho_{\text{TiN}}/t_{\text{TiN}}$, where $\rho_{\alpha\text{-Ti}}$ and ρ_{TiN} are the electrical resistivities, $t_{\alpha\text{-Ti}}$ is the thickness, and t_{TiN} is the combined thicknesses for the α-Ti and TiN films, respectively, are used to obtain Eq. (1).

The values for the properties at 20 °C on the right-hand side of Eq. (1) are available and are listed in Table VII together with their source references. The CTE values are about two to three orders of magnitude smaller than the TCR values. Substituting these values into Eq. (1), the normalized slope of the linear *in situ* R_s vs temperature curve at 20 °C is calculated to be $(1/R_s)(dR_s/dT) = +1880$ ppm/°C. It is very close to the measured value of +1890 ppm/°C in this study.

It is interesting to observe that all of the cooling curves had an identical slope for $T_{\max} = 474$ °C and above. This slope is smaller than that of the heating curves. Since no interaction is expected below 405 °C based on the result obtained from the *in situ* R_s measurement for $T_{\max} = 405$ °C, this reduced slope indicates that the effective temperature coefficient of resistivity (TCR) of the combined $\text{TiN}_{1.12-\delta}/\alpha\text{-Ti(N)/TiN}_{1.12}$ or $\text{TiN}_{1.12-\xi}/\text{Ti}_2\text{N(Ti)/TiN}_{1.12-\xi}$ film stacks is smaller than that of the original $\text{TiN}_{1.12}/\alpha\text{-Ti/TiN}_{1.12}$ film stack.

V. CONCLUSIONS

In the δ-TiN/α-Ti/δ-TiN system, nitrogen dissolves from TiN into α-Ti between 405 and 474 °C. A significant reaction between α-Ti and TiN occurs in the temperature range of 505–548 °C. The reaction product is ϵ-Ti_2N.

ACKNOWLEDGMENTS

We would like to acknowledge the contributions of materials characterization from Carolyn Gordran (AES), Ted Boden (TEM), Sharon Murphy (AFM), and Roger Reyes (SEM). Part of the materials analysis work was contracted out by SEMATECH. We thank Pat DeHaven of IBM at East Fishkill for XRD analysis. Comments on this manuscript by Ramanath Ganapathiraman of University of Illinois and by Cindy Reidsema and Craig Davis of SEMATECH are greatly appreciated. We are also very grateful to Dr. Theodore B. Selover, Jr. of Design Institute for Physical Property Data for his painstaking search for the thermodynamical data on the ϵ-Ti_2N phase through numerous Russian and reference literatures.

[1] V. P. Glushko, V. A. Medvedev, *et al.*, *Thermal Constants of Substances*, Vol. VII, 1st Part (Russian Academy of Sciences, Moscow, 1974), p. 274. Original data from M. P. Morozova and M. M. Kernburg, Zh. Fiz. Khim. (Russ. J. Phys. Chem.) **40**, 1125 (1966).

[2] M. W. Chase, Jr., C. A. Davies, J. R. Downey, Jr., D. J. Frurip, R. A. McDonald, and A. N. Syverud, *JANAF Thermochemical Tables*, 3rd ed., Part II, Cr-Zr, J. Phys. Chem. Ref. Data **14**, Supplement No. 1, 1985, (The American Chemical Society and the American Institute of Physics for National Bureau of Standards, New York, New York, 1986), p. 939.

[3] Same as Ref. 2, p. 1819 and p. 1542.

[4] T. B. Selover, Jr. and Shi-Qing Wang (unpublished).

[5] J.-E. Sundgren, B.-O. Johansson, S.-E. Karlsson, and H. T. G. Hentzell, Thin Solid Films **105**, 367 (1983).

[6] H. A. Wriedt and J. L. Murray, in *Phase Diagrams of Binary Titanium Alloys*, edited by J. L. Murray (ASM International, Metals Park, Ohio 44073, 1987), p. 176.

[7] G. V. Samsonov, Nitrides, translated from Russian by Foreign Technology Division, Air Force Systems Command, Wright-Patterson Air Force Base, Ohio, 9 July, 1970, Rept. No. FTD-MT-24-62-70, p. 26.

[8] Y. Igasaki and H. Mitsuhashi, J. Appl. Phys. **68**, 2439 (1990).

[9] S.-Q. Wang and J. Schlueter (unpublished).

[10] *CRC Handbook of Chemistry and Physics*, edited by D. R. Lide, 72nd ed. (CRC, Boca Raton, 1991).

[11] M. E. Day, M. Delfino, J. A. Fair, and W. Tsai, Thin Solid Films **254**, 285 (1995).

[12] W. Tsai, M. Delfino, J. A. Fair, and D. Hodul, J. Appl. Phys. **73**, 4462 (1993).

[13] G. V. Samsonov and K. I. Portnoy, Alloy Based on High-Melting Compounds, translated from Russian by Foreign Technology Division, Air Force Systems Command, Wright-Patterson Air Force Base, Ohio, 1962, pp. 191–192.